Continuous behavior in a simple model of the adhesive failure of a layer

M. Ferer
Department of Physics, West Virginia University, P.O. Box 6315, Morgantown, West Virginia 26506-6315

Duane H. Smith*
U.S. Department of Energy, Morgantown Energy Technology Center, Morgantown, West Virginia 26507-0880
(Received 14 August 1997)

A fine-scale model of the removal of an adhesive layer by a uniform stress is described. The initial motivation of this modeling project was a description of the removal of a layer of filter cake from cylindrical filters by back-pulse pressure cleaning. The model includes the bonding forces of adhesion between the layer and a substrate, as well as the forces of cohesion between imaginary ''gridblocks'' within the layer. For applied stresses (pressures) greater than a threshold value, some of the layer is removed, with the amount of this failure depending upon the pressure as well as the average adhesive and cohesive forces. The cohesive forces reduce and sharpen the threshold because they increase the stress near broken adhesive bonds. We have performed simulations on a variety of sizes, with the largest being 64 000 gridblocks. Our analysis indicates that the regions of failure are compact with a rough boundary whose perimeter fractal dimension is $D_p = 1.30 \pm 0.05$. In this model, the threshold exhibits the gradual decrease as the system size increases, which is well understood for the general material failure problem in disordered media. Appealing depinning schemes with universal power-law fits of the pressure dependence of the failure rate or the extent of failure are rendered meaningless by the size dependence of the threshold. However, an *ad hoc* fitting scheme provides a reasonably successful collapse of the failure data to a universal curve. [S1063-651X(98)08401-3]

PACS number(s): 62.20.Mk, 81.40.Np, 02.70.Ns, 61.43.Bn

I. INTRODUCTION

In Ref. [1] we presented a model for determining the strength of an adhesive layer under a uniform stress. In this paper we focus on the removal of the layer as a function of stress and time, for smaller thicknesses where the amount of failure (fraction removed) varies continuously with pressure. Material failure is an issue of major importance and therefore has been widely studied for well over a century. Much of this work has naturally focused on the buildup of stress at defects, the formation of cracks, the energy changes during the process, and the dynamics of the crack propagation [2–14]. A number of quasimicroscopic or microscopic models have been used to study these important questions [7–16]. Although similar in spirit to much of this modeling of the fracturing process, our model has two distinct material strengths: an adhesive strength that tries to maintain contact of the layer with the substrate and a cohesive strength that tries to maintain the integrity of the layer. In fact, Ref. [9] studied a very similar model in the limit of very strong adhesion focusing on the failure of the integrity of the layer due to thermal expansion of the substrate [9]. In this paper we allow a variety of cohesive and adhesive strengths. These two effects in the model enable the independent study of various features of material failure, which are less easily disentangled in the more traditional models. The applied stress causes failure at a threshold that scales primarily with the adhesive force. However, the cohesive forces introduce cooperative effects leading to the familiar buildup of stress at defects that both lowers and sharpens the failure threshold. For strong cohesive forces, we observed the familiar first-order-like behavior associated with a steplike threshold [1], where nearly total removal (i.e., failure) occurs above threshold but no failure occurs below threshold. In this paper, we investigate the behavior of the model with weaker cohesive forces where the threshold is continuous so that one might expect behavior similar to that of self-organized criticality (SOC) or depinning transitions.

SOC was proposed to describe apparently robust scale invariance of noise spectra in a number of dynamically unstable systems [17,18]. The proposed scheme enabled the system (most simply viewed as sandpiles at a critical angle of repose) to maintain scale invariance since deviations from the self-organized critical state (as defined by the critical angle) would produce avalanches returning the system continuously to the second-order-like critical state. However, experiments on real sandpiles have been more consistent with discontinuous first-order-like behavior with avalanches on the order of the system size and hysteritic behavior about the angle of repose [19–21].

Power-law noise spectra have been observed with material failure [22,23] and careful simulations have observed SOC-like avalanches [24]. On the other hand, it has long been known that ordinary fracture has a first-order-like threshold with no observable failure below threshold and catastrophic failure above threshold [2]. Recent work on material failure in disordered media has proposed a mean-field theory that both predicted the first-order character of the failure for systems with strong cohesive forces and quantitatively confirmed the results of simulations [25]. With weaker cohesive forces, our model has a continuous threshold similar to the SOC models and we find generic scale invariance in the self-affine fractal behavior of the advance of the rough boundary of the region of failure, similar to the behavior for

*Also at Department of Physics, West Virginia University, WV 26506-6315.

the model avalanches [26] as well as for a number of rough interfaces both for fracture [27] and for fluid invasion [28–30]. In performing power-law fits to the failure rate, which are similar to power-law fits for a number of depinning transitions [31–35], we encountered a problematic size dependence that seems to preclude any useful power-law characterization. It seems likely that this is related to the well-known size dependence of the material failure threshold, where larger systems tend to have larger defects and therefore will have lower failure thresholds [2,36]. Unrelated to these theoretical schemes for extremal dynamics in random media, an *ad hoc* exponential fit leads to an adequate universal collapse of the failure data as a function of pressure and time.

II. DESCRIPTION OF THE FINE-SCALE MODEL

This model was motivated by problems encountered in the removal of the layer of filter cake from cylindrical filters during the back-pulse cleaning cycle of pressurized fluidized bed combustion [1]. In the physical system motivating this model, a layer of filter cake is deposited on a cylindrical candle filter to some thickness t; then a back-pulse pressure is applied from the inside of the candle filter to blow the layer filter cake off, thereby cleaning the filter. The stress or pressure actually responsible for removing the layer is the pressure drop P across the layer. In general, this model describes the strength of a layer adhering to a substrate in the presence of a uniform stress attempting to remove the layer.

In our model, the layer is gridded into rectangular blocks of thickness t and a square $l\times l$ base. The gridding is at a fine scale, intermediate between the centimeter scale of the filter and cake and the micron scale of the individual particles in the layer. Our model system (shown in Fig. 1) is assumed to be flat, lying in the x-y plane; however, continuity around the cylinder is preserved by periodic boundary conditions in the y direction. The other edges are clamped by strong forces to avoid failure initiating at edge defects. The back-pulse cleaning force $F=Pl^2$ is applied at the base of each block; as a result, each block will be displaced by some small amount ϵ in the z direction. The forces resulting from the tensile and shear stresses will balance this applied force. Since the properties of typical filter cake seem to most closely resemble those of a brittle solid rather than a plastic or ductile solid, the forces are assumed to be springlike up to a given threshold strength. Equation (1) presents the relation between the applied force F on a block at $\underline{r}=\frac{1}{2}(i,j)$ (i and j are even integers determining the location along the x and y directions, respectively) and the displacements of that block and the surrounding blocks. Balancing the applied force F are forces due to adhesive springs [providing the forces from tensile stresses multiplied by the area of the base of each block (l^2)] and due to cohesive springs [providing the forces from shear stresses multiplied by the cross-sectional area between any two blocks ($t\times l$)]:

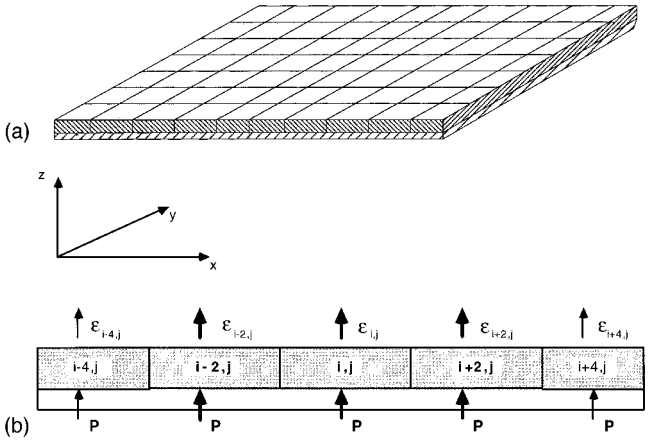

FIG. 1. The gridding of the layer in this model is shown in the upper part of this figure. Griddings of several sizes were used; the largest gridding had 64 000 blocks with 200 units ''around the filter'' (into the page in this figure with periodic boundary conditions connecting the front and back edges) and 320 along its length (the horizontal in this figure). The outward (z direction) applied pressure force P on the filter cake is balanced [see Eq. (1)] by the stresses due to the displacements (ϵ) of the blocks that stretch the cohesive and adhesive springs. Accelerated Gauss-Seidel iterations of Eq. (3) lead to an equilibrium strain field; we have performed iterations until the square of the change in the strain field is less than 10^{-12}. If the actual stress on a bond exceeds its randomly chosen breaking stress, that bond will break.

$$Pl^2=\{l^2\}E_{i,j}\epsilon_{i,j}-\{t\times l\}\{G_{i-1,j}(\epsilon_{i-2,j}-\epsilon_{i,j})+G_{i+1,j}(\epsilon_{i+2,j}-\epsilon_{i,j})+G_{i,j-}(\epsilon_{i,j-2}-\epsilon_{i,j})+G_{i,j+1}(\epsilon_{i,j+2}-\epsilon_{i,j})\}, \tag{1}$$

where E is Young's modulus and G is the shear modulus. Dividing Eq. (1) by l^2, the area of the base, Eq. (1) is simplified with T (the thickness ratio $T=t/l$) replacing t. Note that differences between the average Young modulus $\langle E\rangle$ and the average shear modulus $\langle G\rangle$ can also be absorbed into this thickness factor

$$P=2\langle E\rangle[\underline{E}_{i,j}\epsilon_{i,j}-T\{\underline{G}_{i-1,j}(\epsilon_{i-2,j}-\epsilon_{i,j})+\underline{G}_{i+1,j}(\epsilon_{i+2,j}-\epsilon_{i,j})+\underline{G}_{i,j-1}(\epsilon_{i,j-2}-\epsilon_{i,j})+\underline{G}_{i,j+1}(\epsilon_{i,j+2}-\epsilon_{i,j})\}], \tag{2}$$

where the new thickness parameter incorporates the thickness ratio and the ratio of the shear to Young's moduli $T=(t/l)(\langle G\rangle/\langle E\rangle)$ and the underlined moduli are normalized, i.e., $\underline{E}_{i,j}=E_{i,j}/2\langle E\rangle$ and $\underline{G}_{i,j}=G_{i,j}/2\langle G\rangle$, so that their average value is one-half. Equivalently, the thickness parameter is the ratio of the spring constants of the average ''cooperative'' cohesive force to the average ''single-particle'' adhesive force, providing a relative measure of the cooperative forces in the system. Equation (2) may now be solved for the displacement of any one block (i,j):

$$\epsilon_{i,j}=\frac{T\{\underline{G}_{i-1,j}\epsilon_{i-2,j}+\underline{G}_{i+1,j}\epsilon_{i+2,j}+\underline{G}_{i,j-1}\epsilon_{i,j-2}+\underline{G}_{i,j+1}\epsilon_{i,j+2}\}+\underline{P}}{T\{\underline{G}_{i-1,j}+\underline{G}_{i+1,j}+\underline{G}_{i,j-1}+\underline{G}_{i,j+1}\}+\underline{E}_{i-1,j}}. \tag{3}$$

Given the distributions of normalized moduli and the normalized value of applied pressure $\underline{P}=P/2\langle E\rangle$, one guesses values of the displacements and then iterates Eq. (3) until the displacements stabilize between iterations. If the tensile stress

$$\underline{E}_{i,j}\epsilon_{i,j}>\underline{\sigma}_{\max\, i,j} \tag{4}$$

exceeds the maximum value (breaking strength) for the (i,j) adhesive spring, that spring will break; again in Eq. (4) the stress is normalized in that $\underline{\sigma}_{i,j}=\sigma_{i,j}/2\langle E\rangle$. Similarly, if the shear stress exceeds the breaking strength for the cohesive spring between any two adjacent blocks, e.g.,

$$\underline{G}_{i,j+1}(\epsilon_{i,j}-\epsilon_{i,j+2})>\underline{\tau}_{\max\, i,j+1}, \tag{5}$$

that spring will break.

It is natural to assume that the observed time dependence of the layer removal (on the order of a few milliseconds [37]) is much slower than the elastic relaxation of the layer (e.g., the inverse frequency of elastic waves or the speed of sound, on the order of fractions of milliseconds [38,39]). This justifies a quasistatic process where the layer reaches elastic equilibrium [as given by Eq. (1)] between successive breaking of bonds. The computations in our quasistatic model proceed as follows: (i) With the layer, at equilibrium, under no load, the back-pulse cleaning pressure is applied; (ii) the layer reaches a new elastic equilibrium [Eq. (3) is iterated until stabilization is reached]; (iii) then, at the end of this time step each bond weaker than the actual stress is broken; (iv) steps (ii) and (iii), which together constitute one time step, are repeated, until a final time step at which no further bonds break. Once some bonds have broken at the end of a time step, the nearby bonds will be under a greater stress, increasing the likelihood that they will break at the end of the next time step. In this cascade, more bonds break than would have broken without the interaction mediated by the cohesive bonds. Thus the cooperative effect resulting from the cohesive bonds produces a cascade that lowers and sharpens the threshold.

III. RESULTS

In reality, the layer has definite thickness and the ''cohesive'' forces may be just as significant as the ''adhesive'' forces. Since the ''thickness parameter'' T is the ratio of these two forces (also of the two breaking stresses) in Eqs. (1)–(5), varying T will vary the relative effect and importance of the adhesive and cohesive forces (and strengths). Therefore, the natural variables in our problem are (i) the applied pressure, (ii) the thickness parameter, (iii) the time step, (iv) the length scale, and (v) the distributions of moduli and strengths. To reduce the complexity of the results, we will assume that the applied pressure is constant; the effect of a known time dependence of the pressure can be easily ascertained once the dependence of the failure upon pressure and time has been determined. In all of our simulations, we have chosen a uniform distribution of moduli. Each of the normalized moduli was chosen randomly from a flat distribution between 0 and 1. However, relying on the spring analogy, we assume that thicker bonds between granules in the filter cake will be both stiffer and stronger since they can be mimicked by more springs connecting the granules; for this reason, each normalized breaking strength was strongly correlated with the modulus in that each breaking strength was chosen randomly from a Gaussian distribution that was sharply peaked about the value for that normalized modulus. In our earlier paper for the same broadest distribution, we discussed how increasing the thickness eventually sharpens the threshold to a step (i.e., all of the layer is removed at and above the threshold, while none is removed below threshold [1]). Using a more sharply peaked distribution of forces would only serve to further sharpen this threshold narrowing the range of pressures over which the failure occurs. For two thicknesses $T=\frac{1}{2}$ and 1, which allow continuous layer removal (i.e., the threshold is not steplike), we focus on the dependence of the amount of layer removed as a function of pressure and time as well as on the size dependence of these quantities.

IV. LAYER REMOVAL AS A FUNCTION OF PRESSURE AND TIME

For two thicknesses we have studied the system on a number of length scales for a variety of pressures. From the largest systems, which are 200 blocks wide by 320 blocks long with 64 000 $l\times l$ blocks, to the smallest, which are 60 blocks wide by 80 blocks long with only 4800 $l\times l$ blocks, we have performed simulations for two thickness ratios: $T=\frac{1}{2}$, where the cohesive forces are half as strong as the adhesive forces, and $T=1$, where the cohesive forces are just as strong as the adhesive forces. For a number of systems (different sets of normalized moduli and breaking strengths), the midpoint pressure $P_{\rm mid}$ was determined; the midpoint pressure is the pressure at which half of the layer will be removed. A range of pressures around the midpoint pressure was then scanned and the results were averaged over the different realizations of the system (i.e., differing only in the random choice of strengths and moduli). This modeling demonstrates the effect of thickness and pressure upon the amount of material failure.

Figure 2 shows the time dependence of the amount of failure (mass or number of blocks removed from the layer) by a pressure $dP=P-P_{\rm mid}$ away from the midpoint pressure. For these thicknesses, the amount of failure varies continuously from very little failure to total failure or removal as pressure increases. The time dependence appears to be very similar for both thicknesses. However, it should be noted that the larger thickness has a lower and a sharper threshold, as we discussed in Ref. [1]. Specifically, the midpoint pressure is lower for $T=1$ ($P_{\rm mid}=0.269\,08\pm0.000\,06$) than for $T=\frac{1}{2}$ ($P_{\rm mid}=0.285\,40\pm0.000\,06$); also for the smaller thickness, a larger range of pressures is needed to scan the range from negligible to nearly complete cleaning. In the following section we will fit these failure curves to likely schemes, quantifying the differences between these two thicknesses.

V. FRACTAL CHARACTER OF THE FAILURE PATTERNS

Typical midpoint cleaning patterns for two thicknesses ($T=0.5$ and 1) are shown in Fig. 3. At the midpoint pressure, where half the layer was removed, these figures show the

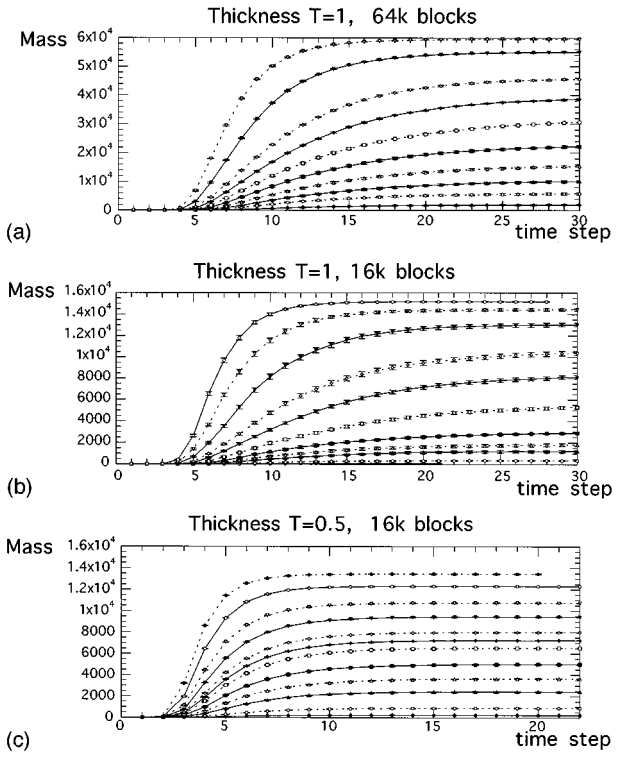

FIG. 2. Filter cake removed as a function of time. These figures show the filter cake removed as a function of time step. As discussed in the text, there is an initial preremoval period when the weaker bonds are being broken; then the filter cake is removed at a particular rate until saturation is achieved at each pressure. It is clear that this mass at saturation M_∞ increases continuously with pressure. (a) Cleaning efficiency for the largest system ($200\times320=64k$ blocks), with thickness parameter $T=1$. Each curve represents the cleaning for a particular overpressure ranging from little cleaning at $P=P_{\rm mid}-0.03$ to nearly total cleaning at $P=P_{\rm mid}+0.03$. Cleaning efficiency for the smaller system ($100\times160=16k$ blocks) for thickness parameters (b) $T=1$ for a range of overpressures from -0.03 to $+0.05$ and (c) $T=\frac{1}{2}$ for a range of overpressures from -0.08 to $+0.05$. Note that for the smaller thickness, a larger range of pressures is required to scan the range of from negligible to complete cleaning.

failure originating at several locations (the darkest areas) and then spreading to nearby blocks. The cooperative nature of the failure process is manifest in this growth from the areas of initial failure since the cohesive bonds cause many bonds to share the stress so that unbroken bonds can compensate for nearby broken bonds. The role of increased cooperative (cohesive) forces is clear from these patterns. For the weaker cohesive forces where a larger pressure is required to remove half of the layer, failure initiates at many more sites because of the larger pressure exceeding more thresholds, but the failure is more localized, advancing much less far than in the $T=1$ system with larger cooperative forces. Qualitatively, this $T=\frac{1}{2}$ pattern is intermediate between the relatively smooth $T=1$ pattern and the site percolation patterns of the negligible cohesion limit [1,40].

Similar to sandpile avalanches, box-counting analysis indicates that these regions of growth are compact with a dimension of $D=2$; however, the boundary of the failure region appears rough, suggesting a self-affine fractal similar to those found in sandpile avalanches, in other slow fracturing processes, and in fluid invasion problems. To determine the fractal dimension of the rough boundary of the failure region, we have determined both the perimeter of the boundary and the mass of the layer removed as a function of pressure and time step for a number of realizations. We then averaged the perimeter length L and mass m over the realizations. For a growing pattern, plotting the perimeter length vs mass will determine the perimeter fractal dimension D_p,

$$L\approx Am^{1/D_p}. \tag{6}$$

Figure 4 shows three of these L vs m plots for all times and for all pressures for the $64k$ block $T=1$ system and the $16k$ $T=1$ and $\frac{1}{2}$ systems. Least-squares fits of Eq. (6) to the three sets of precutoff data predict values of the fractal dimension from 1.32 for the large $T=1$ system to 1.254 for the smaller $T=1$ system. In the power-law regime, before cutoff, all of the data (in addition to data from the 4800 block systems) are consistent with a fractal dimension $D_p=1.30\pm0.05$. To within the uncertainties, this agrees with the fractal dimension from simulations for the perimeter of sandpile avalanches in the self-organized critical state [26]. Furthermore, this is similar to the quantitative behavior of many rough interfaces with a Hurst-roughness exponent of $H=2-D_p=0.70\pm0.05$. It should be emphasized that these are not near threshold data; rather the data are for all pressures and all times. The only data excluded from the power-law fits are those data that manifest obvious finite-size effects, i.e., near the downturn in the plots where the perimeter is approaching the edges of the model.

VI. CHARACTERIZING THE FAILURE FRACTION

A. Size dependence

There are a number of appealing similarities between this adhesive failure model, the more traditional models of self-organized criticality, and the systems with depinning transitions. Our model of adhesive failure has a threshold pressure with a continuous increase in the extent of failure above this threshold. The avalanches in similar fracturing models have been shown to obey SOC-like power laws near the failure threshold [24]. Any quasistatic failure model assumes well-separated time scales between the short times required for approach to elastic equilibrium and the longer times for the propagation of failure [41]. We have found compact failure patterns with a rough perimeter with the same fractal dimension as sandpiles.

However, we find a detailed quantitative comparison with SOC and depinning expectations problematic. It has been long known that real systems have a failure (or fracture) threshold that decreases with size. During the Renaissance, da Vinci conducted experiments that showed that increasing the length of a wire would decrease the strength of the wire [2]. We now understand that since fracture initiates at the largest defect where the stress is greatest, the increased length increased the likelihood of having a larger defect, thereby reducing the load required to initiate failure [2,16]. More recently, careful simulations on random two-dimensional $L\times L$ models have shown that the fracture threshold decreases as a power of $\ln(L)$ [13,42,43]. It has

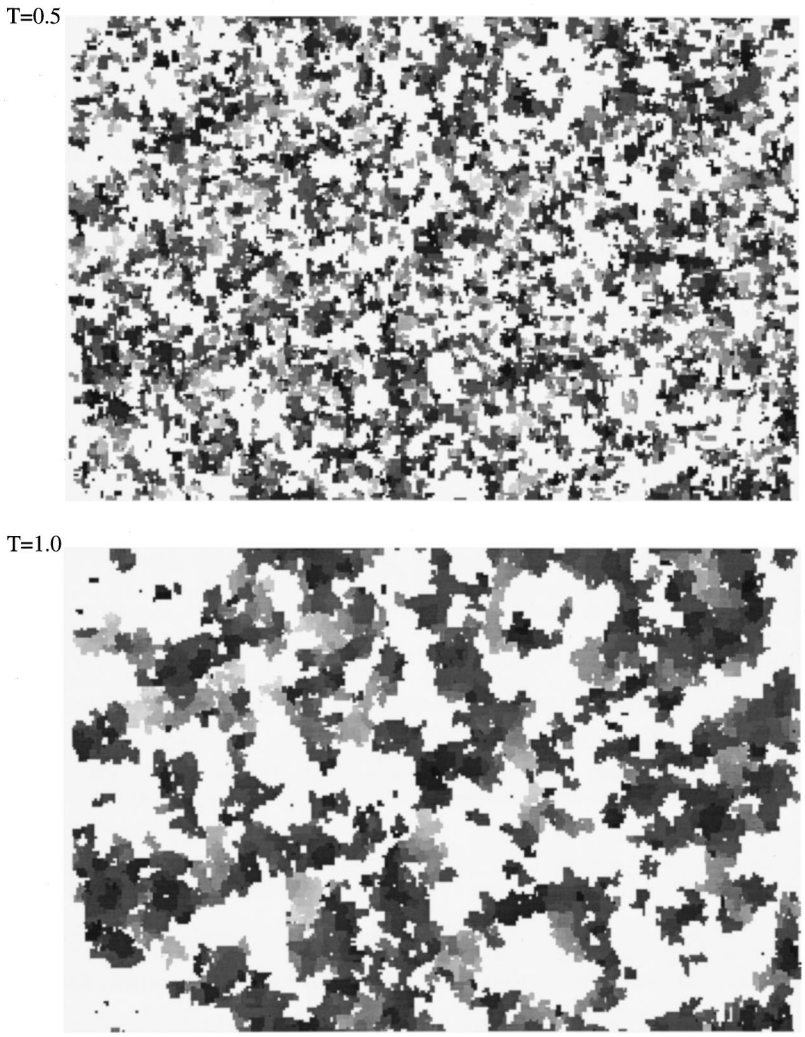

FIG. 3. Typical cleaning patterns for two thicknesses: $T=\frac{1}{2}$ (top) and $T=1$ (bottom). Failure of the layer initiated at the darkest parts and spread to the lighter regime. The larger cooperative (cohesive) forces in the $T=1$ model cause the failure to spread much farther than in the $T=\frac{1}{2}$ model; therefore, removal of half of the layer is accomplished by a lower pressure. Except for the change in thickness, both realizations are identical (i.e., same sets of random numbers, relatively weak bonds in the same locations, etc.).

been shown in the context of percolation theory that the size of the largest defect in a random system increases with the size of the system as $\ln(L)$ [36]. Therefore, the applied force required to initiate failure should decrease as $1/\ln(L)$ since the larger the defect, the greater the local stress and the smaller the applied force required for the local stress to initiate failure [44]. Therefore, as the system approaches an infinite size, the failure threshold will go to zero.

However, because the $\ln(L)$ size dependence is so slow, macroscopic systems are not infinite and experiments on real macroscopic systems show that these systems yield at a finite (i.e., nonzero) threshold. Furthermore, although annealed systems may reduce the number of random defects, thereby raising the threshold, it seems unlikely that random defects can be entirely avoided. Any real material will have some random defects and this randomness will enforce a decrease in threshold with size.

To investigate this size dependence for our adhesive failure model, we have determined the threshold pressure (the pressure at which the first mass of adhesive layer is removed) for a variety of sizes (1000, 4000, 16 000, and 64 000 blocks). A plot of this threshold pressure vs $[\ln(\text{size})]^{-1}$ is shown in Fig. 5. This figure shows that the threshold pressure decreases monotonically with $[\ln(\text{size})]^{-1}$, consistent with the previous discussion of failure in a somewhat different randomized model [42,13,43].

The solid black circles show the average of the threshold pressure for a number of realizations (different random assignments of the bond strengths), whereas the single dots show the threshold for each of the realizations. The horizontal spread in $[\ln(\text{size})]^{-1}$ is an artifact introduced to enable one to more easily distinguish between the different thresholds (dots) for different realizations. The real spread in the threshold pressure shows (i) the significant randomness in the defect size in a given realization and its effect on the threshold, (ii) how small the threshold pressures can be for individual realizations, and (iii) that this scatter in threshold pressure does not decrease significantly with system size. It is entirely consistent with Fig. 5 that the threshold in the present problem would decrease to zero for an infinite system. However, for a macroscopic system (say, size $\approx 10^{20}$), Fig. 5 suggests that the threshold would be nonzero.

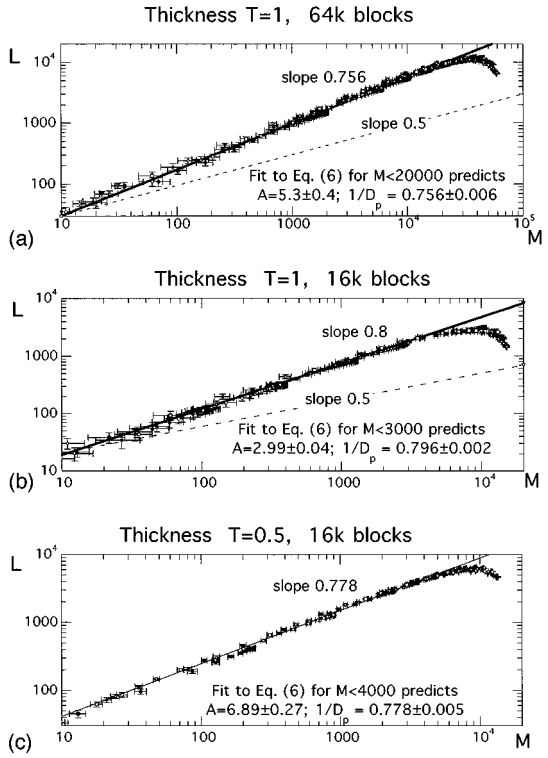

FIG. 4. Three perimeter length (L) vs mass (M) plots for all times and for all the pressures in Fig. 2 for the 64k block $T=1$ system (top), the 16k block $T=1$ system (middle), and the 16k block $T=\frac{1}{2}$ system (bottom). Least-square fits of Eq. (6) to the three sets of pre-cutoff data predicts values of the fractal dimension from 1.32 ± 0.01 for the large $T=1$ system to 1.26 ± 0.01 for the smaller $T=1$ system, with the 16k $T=\frac{1}{2}$model having the intermediate value of 1.285 ± 0.010.

Unlike the previous models where failure, once initiated at threshold, extends through the system, here the extent of failure increases continuously as the pressure is increased above threshold. The size dependence of pressures associated with a given level of failure is very different from the size dependence of the threshold pressure. Contrasting the size

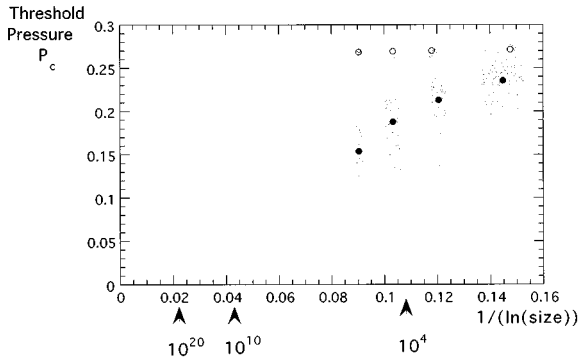

FIG. 5. Threshold pressure and midpoint pressure vs $[\ln(\text{size})]^{-1}$ for $T=1$. The solid black circles show the average of the threshold pressure for a number of realizations (different random assignments of the bond strengths), whereas the small dots show the threshold for each of the realizations. The open circles show the average of the midpoint pressure for a number of realizations (indicated by the small dots).

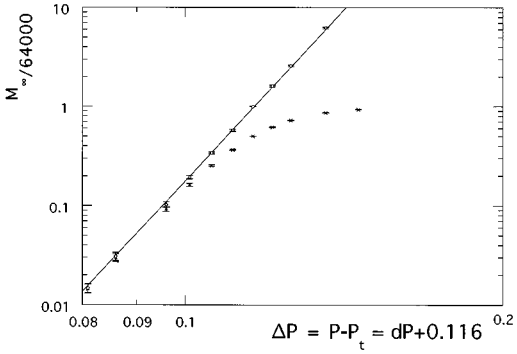

FIG. 6. Fractional amount of eventual failure ($M_\infty/64\,000$) vs $\Delta P=P-P_t=dP+0.116$. Not surprisingly, the failure fraction ($\times$) obeys a power law [Eq. (7)] only for small values of failure fraction ($f<0.1$) with increasing deviations near saturation at $f\simeq1$. Surprisingly, the simplest assumption for a cutoff function $f=\mathcal{F}/(1+\mathcal{F})$ works quite well with this measure of eventual failure $\mathcal{F}=f/(1-f)$ ($\bigcirc$) obeying the same power law for both small and large measures of failure $\mathcal{F}$. The solid line shows the best fit to Eq. (7); $\mathcal{F}=(8.6\Delta P)^{11.475}$.

dependence of the threshold pressure with the size dependence of $P_{\rm mid}$ (the pressure required to remove one-half of the adhesive layer), there is negligible size dependence in $P_{\rm mid}$ and any scatter in $P_{\rm mid}$ between different realizations decreases significantly with system size. Clearly, this midpoint pressure is better characterized for large systems than is the threshold pressure.

B. Pressure dependence

Still, for any given size system, there is a threshold with a continuous increase in the amount of failure (growth in the region of failure) until an interface is reached where the pinning forces (local material strengths) are too great to allow additional failure. This suggests a correspondence with depinning transitions where the rate of advance of an interface increases with applied force above a threshold [45–47]. In any case, the existence of a threshold at P_t with no adhesive failure below the threshold and a continuous growth in the amount of failure with the increase of pressure above threshold naturally suggests a power-law fit $(P-P_t)^\beta$. Figure 6 shows the log-log plot of the fractional amount of failure vs $P-P_t$. Not surprisingly, the failure fraction obeys a power law only for small values of failure fraction ($f<0.1$) with increasing deviations near saturation at $f\simeq1$. Surprisingly, the simplest assumption for a cutoff function $f=\mathcal{F}/(1+\mathcal{F})$ works quite well, with this measure of failure $\mathcal{F}=f/(1-f)$ obeying the same power law for both small $\mathcal{F}$, where $f\simeq\mathcal{F}$, and for large $\mathcal{F}$, where $f\simeq1$. The solid line (in Fig. 6) shows the best power-law fit to $\mathcal{F}$:

$$\mathcal{F}=\{\phi(dP-dP_t)\}^\beta, \tag{7}$$

this best fit has an exponent $\beta\simeq11.5$. Although the theoretical treatments [46,47] of the depinning transition suggest a small value for this exponent $\beta<1$, a simulation on large sandpiles [26] and several experiments on different systems [31–35] all find larger values of β. Several find values of $\beta>2$ [26,32] with one finding a value $\beta\simeq7$, nearly as large as ours [34]. Admittedly, this measure of failure $\mathcal{F}$ is not

TABLE I. Size and thickness dependence of the fitting parameters in Eqs. (7) and (8).

System	ϕ	β	dP_t	A	B
$T=1,(4.8k)$	16.1±0.1	5.2±0.1	0.0609	101±3	9±1
$T=1,(16k)$	12.3±0.1	7.2±0.2	0.0815	97±1	4.9±0.3
$T=1,(64k)$	8.60±0.02	11.475±0.10	0.115	102±1	5.1±0.3
$T=\frac{1}{2},(16k)$	6.94±0.04	5.86±0.05	0.165	39.3±0.6	3.8±0.6

identical to the velocities of the pinned interfaces in the other work. However, the scaling of $\mathcal{F}$ should differ from the scaling of the failure rate $d\mathcal{F}/dt$ only by a characteristic time scale that seems nearly constant. Furthermore, for the compact failure patterns discussed earlier, the rate of growth of failure is directly related to the velocity of the interface bounding the region of failure, and this is very similar to the interfacial velocities in the depinning systems. In any case, we find a large exponent for the increase in damage with increasing pressure, which, like other determinations of β for depinning systems, is significantly larger than the small value predicted by the theoretical treatments [46,47].

It seems likely that the size of this exponent may be affected by the size dependence of the threshold because if the threshold P_t decreases with size while $P_{\rm mid}$ (the pressure at which half the layer is removed) does not change, a larger power will be needed to mimic both the slower removal rate just above the lower threshold and the similar removal rate near $P_{\rm mid}$. Indeed power-law fits to our smaller systems require smaller values of the exponent β; specifically the best fits to the data predict $\beta\approx 7.2$ for the $16k$ systems and $\beta \approx 5.2$ for the $4.8k$ systems; see Table I. This nontrivial size dependence for the threshold and the exponent precludes a universal prediction for the power law applicable to macroscopic systems. In fact, in the thermodynamic limit of infinite system size, a power-law fit for these random systems seems meaningless.

On the other hand, the size dependence of the removal of finite fractions (of finite measures of failure $\mathcal{F}$, i.e., not close to threshold) seems well behaved and easily characterizable. Figure 7 shows the measure of failure $\mathcal{F}$ vs $dP=P-P_{\rm mid}$ for systems of three different sizes ($64k$, $16k$, and $4.8k$). The

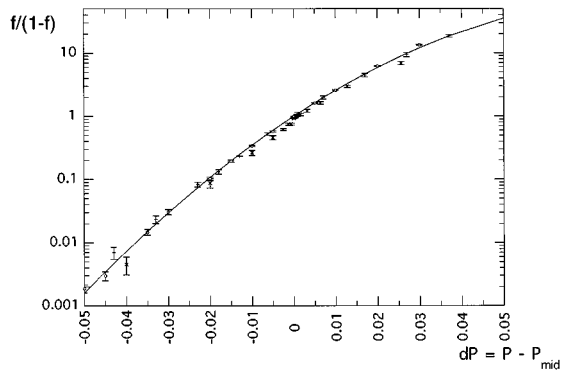

FIG. 7. Measure of eventual failure $\mathcal{F}$ vs $dP=P-P_{\rm mid}$ for the $T=1$ systems of three different sizes [$64k$ (○), $16k$ (+), and $4.8k$ (×)]. The only observable deviations occur at the smallest measures of failure. The *ad hoc* exponential form (8) provides a reliable fit to the well-characterized, size-independent finite failure regime; the solid line shows this best fit $\mathcal{F}=\exp[102dP(1-5.1dP)]$.

only observable deviations occur at the smallest failure, suggesting that the pressure dependence of the finite measures of failure has a well-defined thermodynamic limit. Just as a small power law suggests a possible logarithmic dependence, a large power law suggests an exponential dependence, implying that $\ln\mathcal{F}$ might have a simple dependence on dP, e.g., a polynomial. Figure 7 shows simple nearly linear behavior that is well fit by the quadratic shown

$$\mathcal{F}=e^{AdP(1-BdP)}. \tag{8}$$

Note that at $dP=0$, $P=P_{\rm mid}$, so that $\mathcal{F}=1$, eliminating the need for a constant in the quadratic $AdP-ABdP^2$. Table I shows the values from the best fits of both Eqs. (7) and (8) to the data, and the corresponding size dependence. The exponential fits show an insignificant size dependence and are all consistent with the values chosen for the fit in Fig. 7.

Although the power-law fits above threshold seem more fundamental and physically meaningful, the size dependence seems to preclude a meaningful power-law fit to finite systems. On the other hand, the seemingly *ad hoc* exponential fits offers more promise of providing a useful fit to macroscopic systems, given the negligible size dependence in the parameters fitting the simulation results.

C. Dependence on pressure and time

It is natural to hope that the failure fraction might be described as a function of the two variables

$$\mathcal{F}/\mathcal{F}(P)=\mathfrak{F}(t/\tau(P)), \tag{9}$$

where, in addition to the above pressure dependence of the measure of failure there is a pressure-dependent characteristic time that affects the pressure dependence of the rate of cleaning. Preliminary to ascertaining the pressure dependence of this characteristic time, Fig. 8 shows the time dependence of $\mathcal{F}/\mathcal{F}(P)$. Surprisingly, these curves overlap to within the rather large uncertainties; any effort to look for a characteristic time seems meaningless, with the effect of the characteristic time being negligible compared to the errors in the fitting function $\mathcal{F}(P)$. The careful reader may have noticed that the smallest pressure data have been omitted from these plots simply because of their large uncertainties. On the other hand, the largest pressures have also been omitted primarily because the fitting function $\mathcal{F}(P)$ is less successful at the extremes, but also because the highest pressure data exhibit a noticeably sharper failure rate (sharper shoulder) than the other data. In any case, the reliable data above but not too far above threshold can be moderately successfully represented by a universal function with negligible size dependence since the exponential fits to $\mathcal{F}(P)$ will accommodate both the $64k$ and the $16k$ data (Fig. 8). If there is a

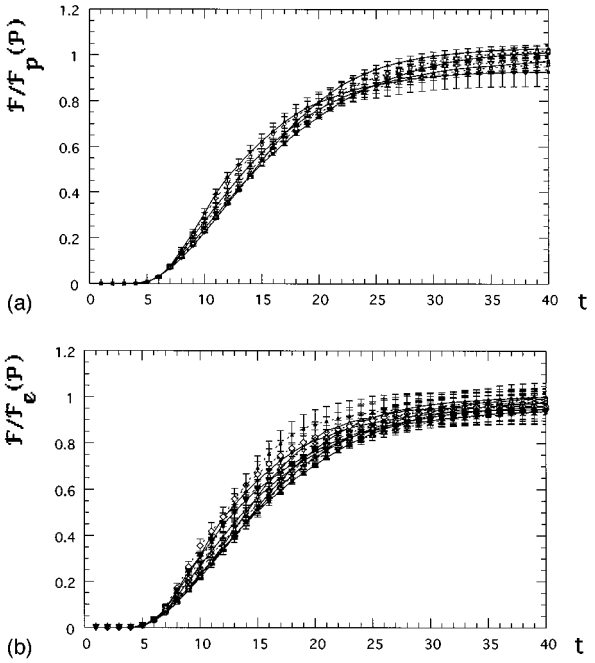

FIG. 8. For thickness $T=1$, plots of normalized measure of failure $\mathcal{F}/\mathcal{F}(P)$ (a) for the power-law form of $\mathcal{F}_p(P)$ for the 64k system ($dP=-0.02$ to 0.01) and (b) the *ad hoc* exponential form of $\mathcal{F}_e(P)$ for both the 64k ($dP=-0.02$ to 0.01) and 16k ($dP=-0.005$ to 0.04) systems. Any pressure dependence of a characteristic time is quite weak, being overwhelmed by the strong pressure dependence of $\mathcal{F}(P)$ and small discrepancies in this fit, although the larger overpressures (e.g., for 16k $dP=0.04$, the solid triangles on the dashed line) do show a sharper knee in (b).

pressure-dependent characteristic time its pressure dependence is quite weak, being overwhelmed by the strong pressure dependence of $\mathcal{F}(P)$. On the other hand, Fig. 9 for the smaller thickness ($T=\frac{1}{2}$) shows that the thickness parameter significantly affects the time dependence of the failure with the approach to saturation occurring in many fewer time steps, largely because of the larger pressures required.

VII. CONCLUSIONS

We have performed simulations on a quasistatic model of material failure, which enables one to separately adjust the single-particle (adhesive) forces that scale the failure threshold and the cooperative (cohesive) forces that provide the characteristic buildup of stress at defects, which is responsible for catastrophic failure at larger values of the cohesive force. For the small cooperative forces studied in this paper, the threshold in continuous (second-order-like); however,

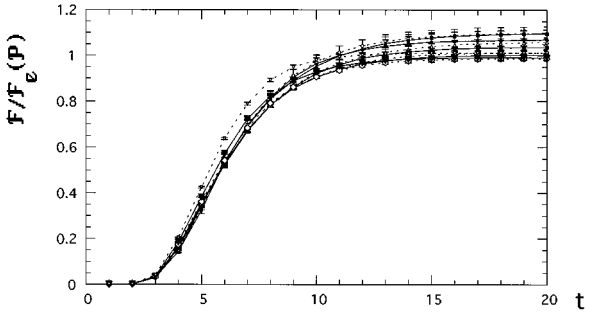

FIG. 9. For thickness $T=\frac{1}{2}$, plots of normalized measure of failure $\mathcal{F}/\mathcal{F}_e(P)$ using the *ad hoc* exponential form of $\mathcal{F}_e(P)$ for the 16k systems ($dP=-0.06$ to 0.035) excluding only the $dP=-0.08$ and 0.05 overpressures. Although there is little evidence for a pressure dependence in a characteristic time, the effect of thickness is clear, with the failure in this thinner system occurring much more rapidly than in the thicker system of Fig. 8.

even these weak cohesive forces have dramatically lowered and sharpened the threshold from the case with zero cohesive forces where the threshold mimics the uniform distribution of the strengths with midpoint pressure of one-half and slope [A of Eq. (8)] unity:

$$T=0.0,\quad P_{\mathrm{mid}}=0.5,\quad A=1,$$

$$T=0.5,\quad P_{\mathrm{mid}}=0.285\,40\pm0.000\,06,\quad A\approx40,$$

$$T=1.0,\quad P_{\mathrm{mid}}=0.269\,08\pm0.000\,06,\quad A\approx100.$$

The region of failure is compact, but the perimeter bounding the region of failure is rough with a perimeter fractal dimension $D_p=1.30\pm0.05$ not just for one state but for the full range of pressures, times, and sizes studied. This model exhibits the size dependence of the threshold known to be generic for material failure in disordered systems. This size dependence eliminates the possibility of universal power-law dependence of the failure or failure rate upon pressure above threshold. However, the midpoint pressure has a well-defined thermodynamic limit. *Ad hoc* exponential fits of the amount of material failure to deviations from this midpoint pressure exhibit little size dependence and offer the hope of well-characterized extensions to systems of macroscopic size. An interesting feature of the model is the transition to first-order behavior (steplike thresholds) for larger cohesive forces [1]. This transition will be investigated elsewhere.

ACKNOWLEDGMENT

We gratefully acknowledge the support of the U.S. Department of Energy, Office of Fossil Energy.

[1] M. Ferer and D. H. Smith, J. Appl. Phys. **81**, 1737 (1997).
[2] V. Z. Parton, *Fracture Mechanics: From Theory to Practice* (Gordon and Breach, Philadelphia, 1992).
[3] A. A. Griffith, Philos. Trans. R. Soc. London, Ser. A **221**, 163 (1920).
[4] B. Cotterell and J. R. Rice, Int. J. Fract. **16**, 155 (1980).
[5] A. Munjiza, D. R. J. Owen, and N. Bicanic, Engineering Computations **12**, 145 (1995).
[6] W. Fenghui, Z. Xuilin, and L. Mingxu, Int. J. Fract. **70**, R19 (1995).
[7] H. J. Hermann and S. Roux, *Statistical Models for the Fracture of Disordered Media* (North-Holland, Amsterdam, 1990).

[8] Y. Termonia and P. Meakin, Nature (London) **320**, 429 (1986); P. Meakin, Science **252**, 226 (1991).
[9] K. M. Crosby and R. M. Bradley, Phys. Rev. E **55**, 6084 (1997).
[10] E. Louis and F. Guinea, Europhys. Lett. **3**, 871 (1987).
[11] H. Furukawa, Phys. Rev. E **52**, 5124 (1995).
[12] H. J. Hermann, A. Hansen, and S. Roux, Phys. Rev. B **39**, 637 (1989).
[13] P. M. Duxbury, P. L. Leath, and P. D. Beale, Phys. Rev. B **36**, 367 (1987).
[14] E. S. C. Ching, J. S. Langer, and H. Nakanishi, Phys. Rev. Lett. **76**, 1087 (1996).
[15] L. Golubovic, A. Peredera, and M. Golubovic, Phys. Rev. E **52**, 4640 (1995).
[16] L. Golubovic and A. Peredera, Phys. Rev. E **51**, 2799 (1995).
[17] P. Bak, C. Tang, and K. Wiesenfeld, Phys. Rev. Lett. **59**, 381 (1987).
[18] P. Bak, C. Tang, and K. Wiesenfeld, Phys. Rev. A **38**, 364 (1988).
[19] H. Ceva and R. P. J. Perazzo, Phys. Rev. E **48**, 157 (1993).
[20] G. Held, D. Solina II, D. Keane, W. Haag, P. Horn, and G. Grinstein, Phys. Rev. Lett. **65**, 1120 (1990).
[21] S. R. Nagel, Rev. Mod. Phys. **64**, 321 (1992).
[22] A. Petri, G. Paparo, A. Vespignani, A. Alippi, and M. Costantini, Phys. Rev. Lett. **73**, 3423 (1994).
[23] G. Cannelli, R. Cantelli, and F. Cordero, Phys. Rev. Lett. **70**, 3923 (1993).
[24] G. Caldarelli, F. D. DiTolla, and A. Petri, Phys. Rev. Lett. **77**, 2503 (1996).
[25] S. Zapperi, P. Ray, H. E. Stanley, and A. Vespignani, Phys. Rev. Lett. **78**, 1408 (1997).
[26] P. Grassberger and S. S. Manna, J. Phys. (Paris) **51**, 1077 (1990).
[27] K. J. Maloy, A. Hansen, E. L. Hinrichsen, and S. Roux, Phys. Rev. Lett. **1992**, 213 (1992).
[28] M. Ferer and D. H. Smith, Phys. Rev. E **49**, 4114 (1994).
[29] V. K. Horvath, F. Family, and T. Vicsek, J. Phys. A **24**, L25 (1991).
[30] M. A. Rubio, C. A. Edwards, A. Dougherty, and J. P. Gollub, Phys. Rev. Lett. **63**, 1685 (1989).
[31] S. Kumar, D. Reich, and M. O. Robbins, Phys. Rev. E **52**, R5776 (1995).
[32] J. P. Stokes, M. J. Higgins, A. P. Kushnick, S. Bhattacharya, and M. O. Robbins, Phys. Rev. Lett. **65**, 1885 (1990).
[33] S. Bhattacharya and M. J. Higgins, Phys. Rev. Lett. **70**, 2617 (1993).
[34] T. Delker, D. B. Pengra, and P.-z. Wong, Phys. Rev. Lett. **76**, 2902 (1996).
[35] S. Bhattacharya, M. J. Higgins, and J. P. Stokes, Phys. Rev. Lett. **63**, 1503 (1989).
[36] J. Machta and R. A. Guyer, Phys. Rev. B **36**, 2142 (1987).
[37] S. Laux, B. Giernoth, H. Bulak, and U. Renz, in *Aspects of Pulse-Jet Cleaning of Ceramic Filter Elements*, Proceedings of the 12th International Conference on Fluidized Bed Combustion, San Diego, 1993, edited by Lynn Rubow (American Society of Mechanical Engineers, New York, 1993).
[38] J. S. Langer and H. Nakanishi, Phys. Rev. E **48**, 439 (1993).
[39] F. Abraham, D. Brodbeck, R. Rafey, and W. Rudge, Phys. Rev. Lett. **73**, 272 (1994).
[40] D. S. Stauffer, *Introduction to Percolation Theory* (Taylor and Francis, Philadelphia, 1985).
[41] G. Grinstein, *Scale Invariance, Interfaces, and Non-Equilibrium Dynamics*, edited by A. McKane, M. Droz, J. Vannimenus, and D. Wolf (Plenum, New York, 1995).
[42] L. de Arcangelis, S. Redner, and H. J. Hermann, J. Phys. (France) Lett. **46**, 1585 (1985).
[43] P. M. Duxbury, P. D. Beale, and P. L. Leath, Phys. Rev. Lett. **57**, 1052 (1986).
[44] B. Kahng, G. G. Batrouni, and S. Redner, J. Phys. A **20**, L827 (1987).
[45] J. Koplik and H. Levine, Phys. Rev. B **32**, 280 (1985).
[46] T. Natterman, S. Stepanow, L. Tang, and H. Leschorn, J. Phys. II **2**, 1483 (1992).
[47] O. Narayan and D. S. Fisher, Phys. Rev. B **48**, 7030 (1993).